2019학년도 자연과학대학 학부생 연구 인턴십

【중간( ), 결과(O)】보고서

○ 연구주제(제목) : Prediction of Ground Motions in the Southeastern Korean Peninsula for Scenario Earthquakes in Northern Kyushu

○ 제출자(소속, 학번, 이름): 물리천문학부 2013-10969 이재석

○ 지도교수: 이준기 (인)

==========

=======

본문 내용은 11포인트, 3장 이상 작성할 것

Prediction of Ground Motions in the Southeastern Korean Peninsula for Scenario Earthquakes in Northern Kyushu

Jaeseok Lee

Department of Physics & Astronomy, Seoul National University, Seoul, Korea

August 26, 2019

I. INTRODUCTION

Following the 2016 Mw 7.0 Kumamoto earthquake, possible earthquake scenarios in northern Kyushu area are of concern in seismic hazard analysis of the southeastern Korean Peninsula. Numerous active fault zones including the Kego fault zone or the Kikugawa fault zone are in proximity of 200 km from populated areas such as Busan, and the occurrence of a large earthquake in these fault zones may result in reasonable ground motion. Empirical ground motion prediction equations (GMPEs) are often used in probabilistic seismic hazard analysis (PSHA) to predict intensity of ground motions, yet there are limitations of not being able to account for specific source effects or the velocity structure of an area. Ground motion prediction through simulation-based waveform modelling have several advantages over GMPEs in this aspect, because scenario-specific source effects and 3D velocity structure are explicitly considered in computation of site-specific full three-component waveforms (Song et al., 2014).

Fig 1. Active fault zones at northern Kyushu, Japan in proximity to southeastern Korean Peninsula (NIED - http://www.j-shis.bosai.go.jp/map/)

The goal of this research is to propose a possible earthquake rupture scenario at northern Kyushu and analyze the numerically simulated ground motion at southern Korean Peninsula, which may provide quantitative estimations on structural damages and suggest guidance on preventive measurements for large overseas earthquakes near the Korean Peninsula. Yet in order to accurately reproduce the features of seismic wave propagation and ground shaking through waveform modelling, realistic implementation of both the earthquake source and the velocity model is necessary. Therefore as a preliminary study, this paper will examine the validness of waveform modelling through simulation of past earthquake events rather than focus on the formulation of earthquake rupture scenarios. Fully 3-D seismic wave propagation of the 2005 Fukuoka earthquake and the 2016 Kumamoto earthquake finite fault models are calculated through spectral element method at frequencies up to 0.92 Hz in a 3-D velocity structure with surface topography. Synthetic waveforms and peak ground velocity values across the southern Korean Peninsula are compared with observations and GMPEs. Further tasks to be solved including the formulation of possible earthquake rupture scenarios through pseudo-dynamic modelling are listed along with conclusions.

II. METHODS

2.1. Earthquake Source Model

A. 2005 Fukuoka Earthquake

The 2005 Fukuoka earthquake is a M_W 6.6 strike-slip earthquake that occured on 20 March, 2005 at northwest segment of the Kego fault. The finite fault model of the Fukuoka earthquake is obtained through kinematic inversion of strong motion seismograms (Asano & Iwata, 2006). The size of the finite fault model is 26 km by 18 km, constituted of 117 square subfaults with size 2 km by 2 km. Location of the hypocenter is 33.75 °N , 130.16 °E at depth 14 km with strike 122 °, dip 87 °, and rake angle variations of 1.4 ± 45 °. The moment rate functions of each subfault are given as a series of 6

smoothed ramp functions which has the rise time of 1.0 s separated by 0.5 s. The finite fault model is expressed as 6 consecutive point-source solution with Gaussian source time function on each subfault for calculations in SPECFEM3D.

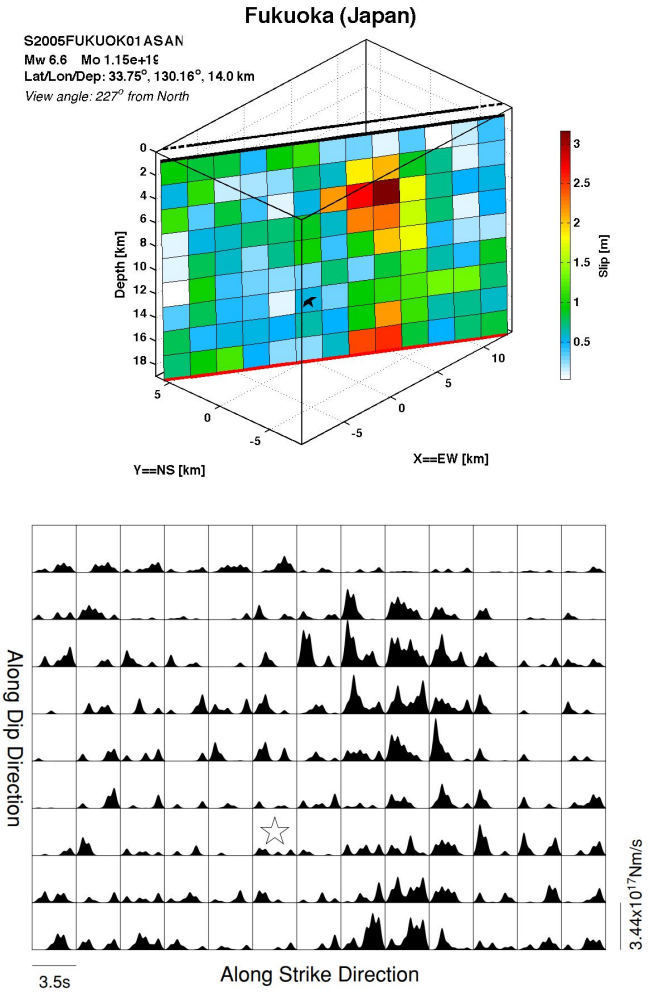

Fig 2. Finite fault model for the 2005 Fukuoka earthquake (above) and moment rate functions for each subfault (below) (Asano & Iwata, 2006).

B. 2016 Kumamoto Earthquake

The M_W 7.0 Kumamoto earthquake occured on 14 April, 2016 at northern part of the Hinagu fault. The finite fault model of the Kumamoto earthquake is also obtained through kinematic inversion of strong motion seismograms (Asano & Iwata, 2016). The finite fault model is composed of two fault segments with length and width of 14 km by 18 km and 28 km by 18 km, divided into 2 km by 2 km square subfaults. Location of the hypocenter is 32.7545 °N , 130.7630 °E at depth 12.45 km. Fault segment 1 has strike 205 °, dip 72 ° and fault segment 2 has strike 235 °, dip 65 ° with rake angle variations of -142 ± 45 ° in both segments. The moment rate functions of each subfault are given as a series of 9 smoothed ramp functions which has the rise time of 1.0 s separated by 0.5 s. The finite fault model is expressed as 9 consecutive point-source solution with Gaussian source time function on each subfault for calculations in SPECFEM3D.

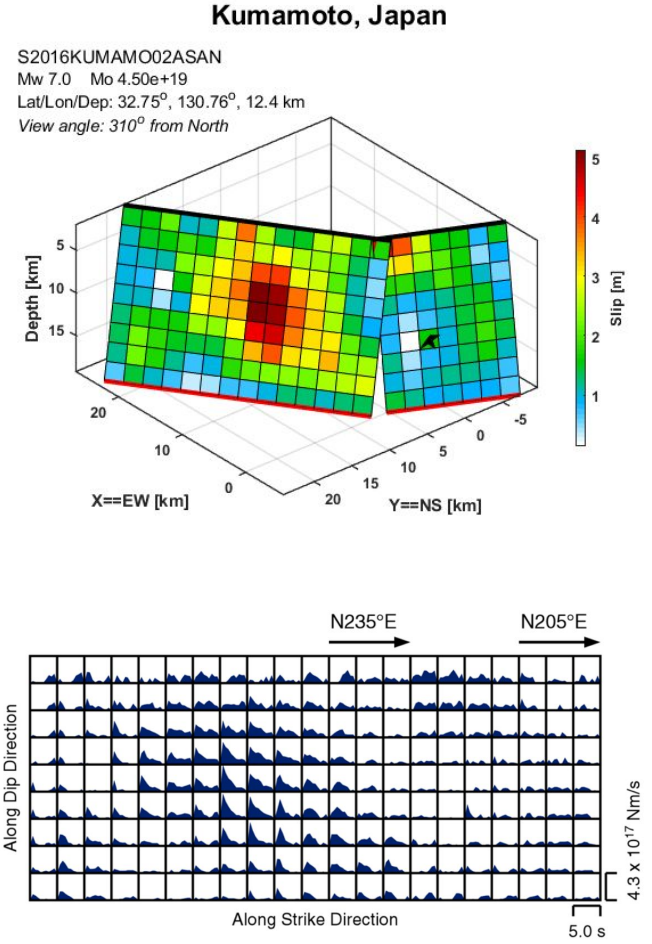

Fig 3. Finite fault model for the 2016 Kumamoto earthquake (above) and moment rate functions for each subfault (below) (Asano & Iwata, 2016).

2.2. Ground Motion Prediction

Ground motion across the southeastern Korean Peninsula resulting from each finite fault models are calculated by spectral element method implemented in SPECFEM3D (Komatitsch & Tromp, 1994). The spectral element method divides the area of seismic wave propagation into non-overlapping hexahedral volume elements as in finite element method. The equation of motion for continuum mechanics at each volume element is expressed as sum of Lagrange polynomials at Gauss-Lobatto-Legendre points. The weak-formulated equation of motion is converted as

diagonalized matrix form of second order ordinary differential equation by Gauss-Lobatto-Legendre integration law, which can be solved numerically by finite difference method.

The 3-D velocity structure of East Asia is inferred from transdimensional Bayesian ambient noise tomography (Kim et al., 2016). The mesh block covers area of latitude 30 °N to 40 °N and longitude 124 °E to 136 °E with depth 80 km, including the whole Korean Peninsula and Kyushu area. The mesh is divided into 2 km regular hexahedral grids which enables maximum frequency computation of 0.92 Hz. Full 3-component waveforms are calculated at F-net, Hi-net, Korea Meteorological Administration (KMA), and Korea Institute of Geoscience and Mineral Resources (KIGAM) seismic stations and compared with observations. Peak ground velocity across the Korean Peninsula for both earthquakes are also calculated and compared with observations and GMPEs for South Korean Peninsula (Emolo et al., 2015) . The synthetic waveforms are computed upto 250 s for the 2005 Fukuoka earthquake and 300 s for the 2016 Kumamoto earthquake with time interval of 0.005 seconds.

III. RESULTS & DISCUSSION

3.1. Seismic Waveform Analysis

The synthetic waveforms and observations are compared at all three radial, tangential and vertical components, both in displacement and velocity. The seismograms are bandpassed between 0.02 to 0.1 Hz and 0.05 to 1 Hz by Butterworth filter and compared separately. The seismograms for only JJU and TJN stations are presented in this paper from **Fig 4** through **Fig 11**.

Overall, the synthetic waveforms fit the observations to a certain extent. The arrival times of body wave phases are generally in agreement, and the phase and wavelength of the seismograms are especially in accordance at the tangential component Love wave. There are some misfits in the waveform of P-SV wave or the Rayleigh wave compared to the Love wave, which is unexpected because the 3-D velocity structure of East Asia in this calculation is obtained from group and phase velocity measurements of Rayleigh wave fundamental modes. The misfits are also larger in high frequency (0.05 ~ 1 Hz) bandpass compared to low frequency (0.02 ~ 0.1 Hz) bandpass. Both seismic attenuation and the effect of the East Sea on seismic wave propagation may contribute to misfits in high frequency.

In both 2005 Fukuoka earthquake and 2016 Kumamoto earthquake, the amplitude of the tangential components are substantially larger compared to radial and vertical components since the earthquake events are mostly strike-slip. The amplitude of synthetic waveforms from 2016 Kumamoto earthquake are 2 ~ 3 times larger than synthetic waveforms from 2005 Fukuoka earthquake because the seismic moment is larger by a factor of about 4.

A problem that needs to be addressed is that the velocity seismograms do not fit in either 2005 Fukuoka earthquake or the 2016 Kumamoto earthquake calculations even though the displacement seismograms seem to be in agreement. The synthetic waveforms and observation are in discordance especially at velocity seismograms of high frequency (0.05 ~ 1 Hz). This problem is critical because accurate velocity computation at high frequency is necessary for PGV prediction and structural damage estimation. Small spike-like noises that are observed in the synthetic displacement seismograms become amplified when differentiated into velocity seismograms, resulting in such high discordance. The cause of this discordance in the velocity seismogram is yet to be identified, whether it results from the velocity structure, source effects, or is a numerical error.

3.2 Peak Ground Velocity

Peak ground velocity values across the Korean Peninsula is calculated and compared with observations for both 2005 Fukuoka earthquake and 2016 Kumamoto earthquake in **Fig 12** and **Fig 13**. The synthetic distribution of PGV is generally in agreement with the observations, with relatively high PGV values at the southeastern tip and the southwestern inland area of the Korean Peninsula. The reason for agreement despite the discordance in velocity seismograms may be because the tangential component waveforms, which have larger amplitude and contribute more to PGV are in agreement.

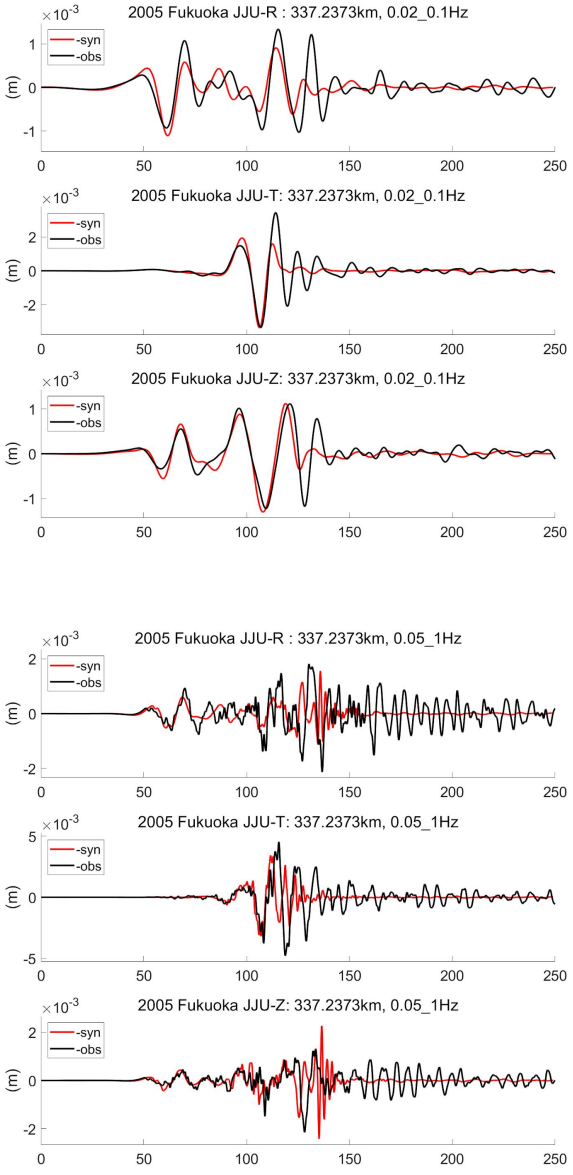

Fig 4. Radial, tangential, and vertical component of synthetic (red) and observation (black) displacement seismogram at JJU station for 2005 Fukuoka earthquake, bandpassed at 0.02 ~ 0.1 Hz (above) and 0.05 ~ 1 Hz (below).

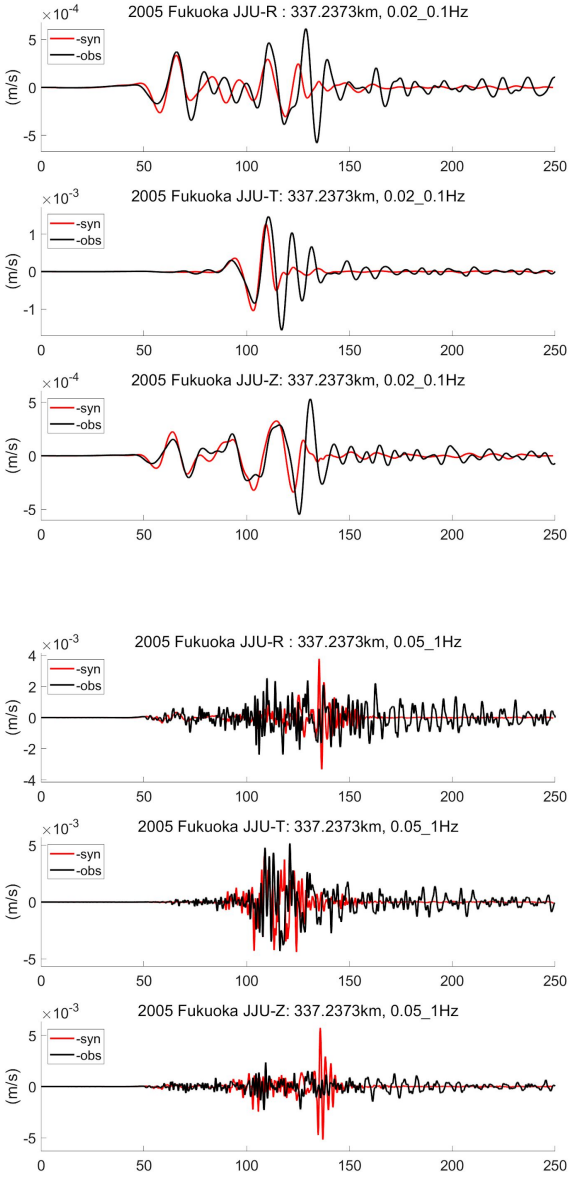

Fig 5. Radial, tangential, and vertical component of synthetic (red) and observation (black) velocity seismogram at JJU station for 2005 Fukuoka earthquake, bandpassed at 0.02 ~ 0.1 Hz (above) and 0.05 ~ 1 Hz (below).

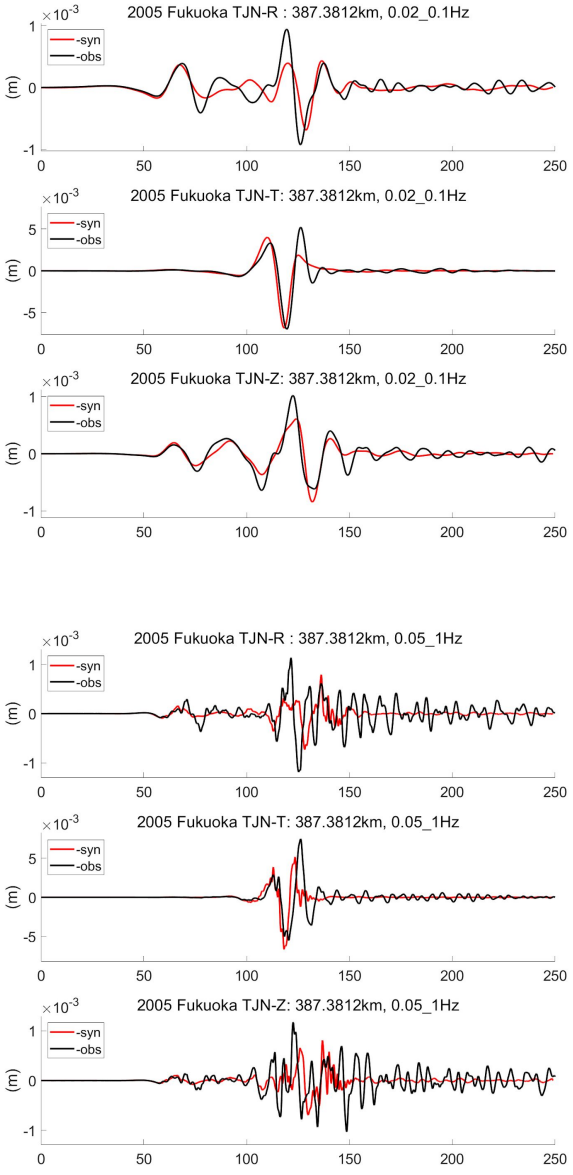

Fig 6. Radial, tangential, and vertical component of synthetic (red) and observation (black) displacement seismogram at TJN station for 2005 Fukuoka earthquake, bandpassed at 0.02 ~ 0.1 Hz (above) and 0.05 ~ 1 Hz (below).

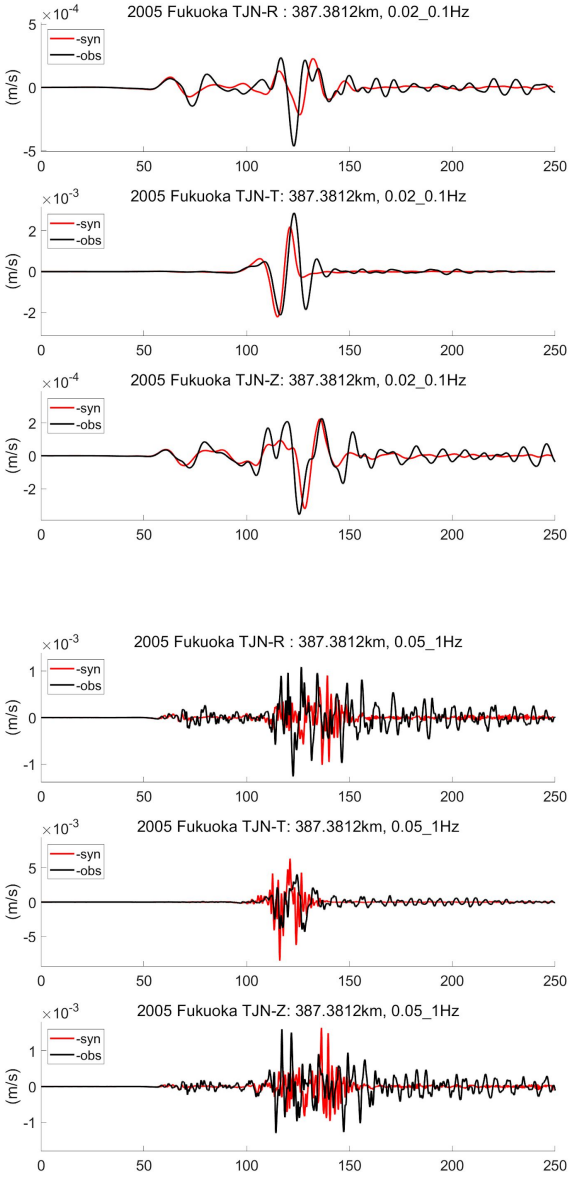

Fig 7. Radial, tangential, and vertical component of synthetic (red) and observation (black) velocity seismogram at TJN station for 2005 Fukuoka earthquake, bandpassed at 0.02 ~ 0.1 Hz (above) and 0.05 ~ 1 Hz (below).

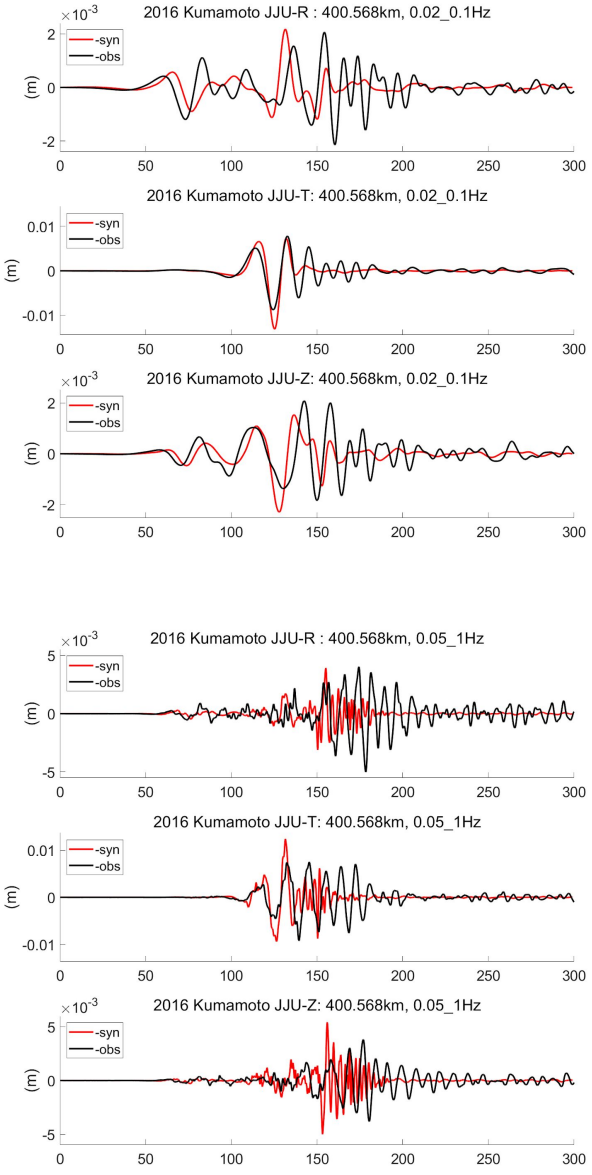

Fig 8. Radial, tangential, and vertical component of synthetic (red) and observation (black) displacement seismogram at JJU station for 2016 Kumamoto earthquake, bandpassed at 0.02 ~ 0.1 Hz (above) and 0.05 ~ 1 Hz (below).

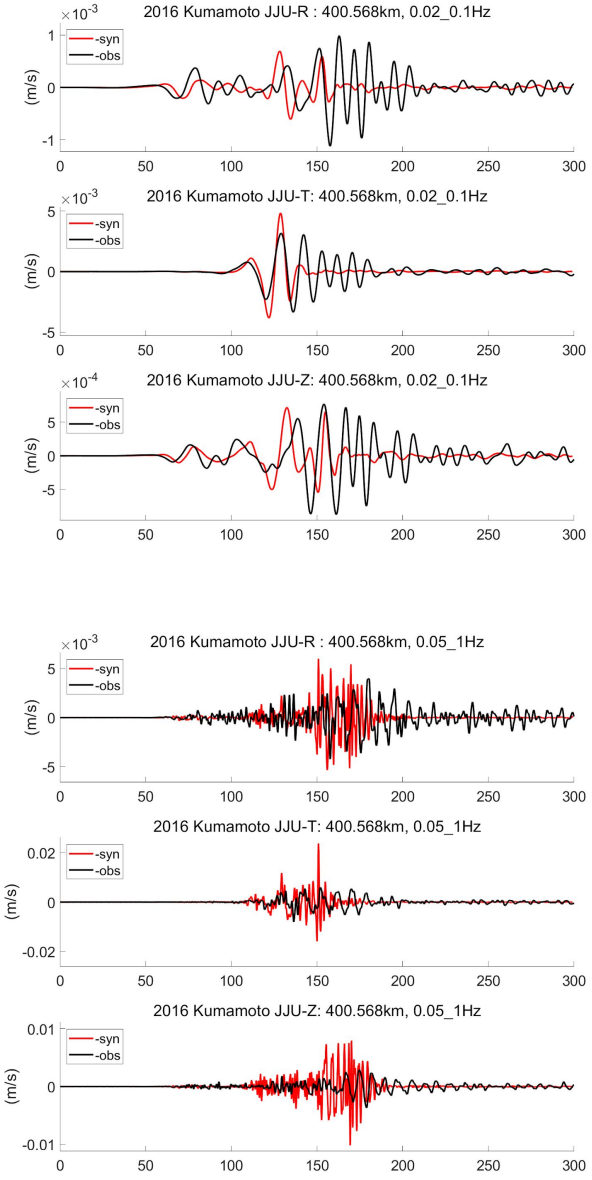

Fig 9. Radial, tangential, and vertical component of synthetic (red) and observation (black) velocity seismogram at JJU station for 2016 Kumamoto earthquake, bandpassed at 0.02 ~ 0.1 Hz (above) and 0.05 ~ 1 Hz (below).

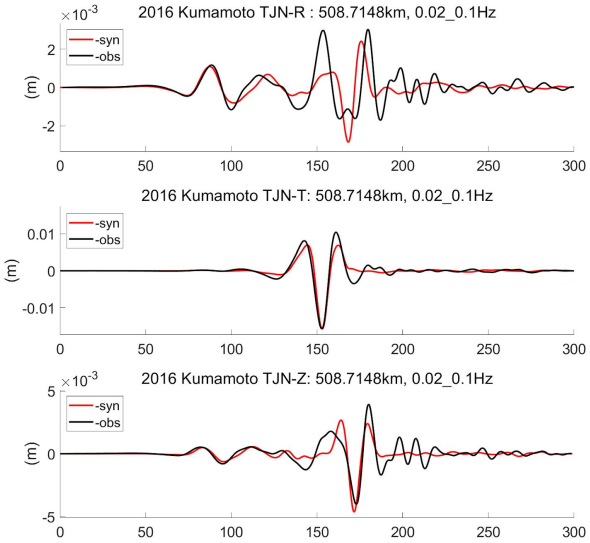

Fig 10. Radial, tangential, and vertical component of synthetic (red) and observation (black) displacement seismogram at TJN station for 2016 Kumamoto earthquake, bandpassed at 0.02 ~ 0.1 Hz (above) and 0.05 ~ 1 Hz (below).

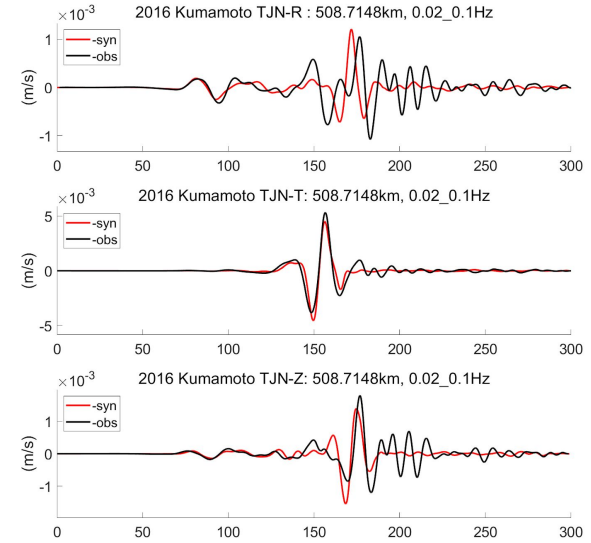

Fig 11. Radial, tangential, and vertical component of synthetic (red) and observation (black) velocity seismogram at TJN station for 2016 Kumamoto earthquake, bandpassed at 0.02 ~ 0.1 Hz (above) and 0.05 ~ 1 Hz (below).

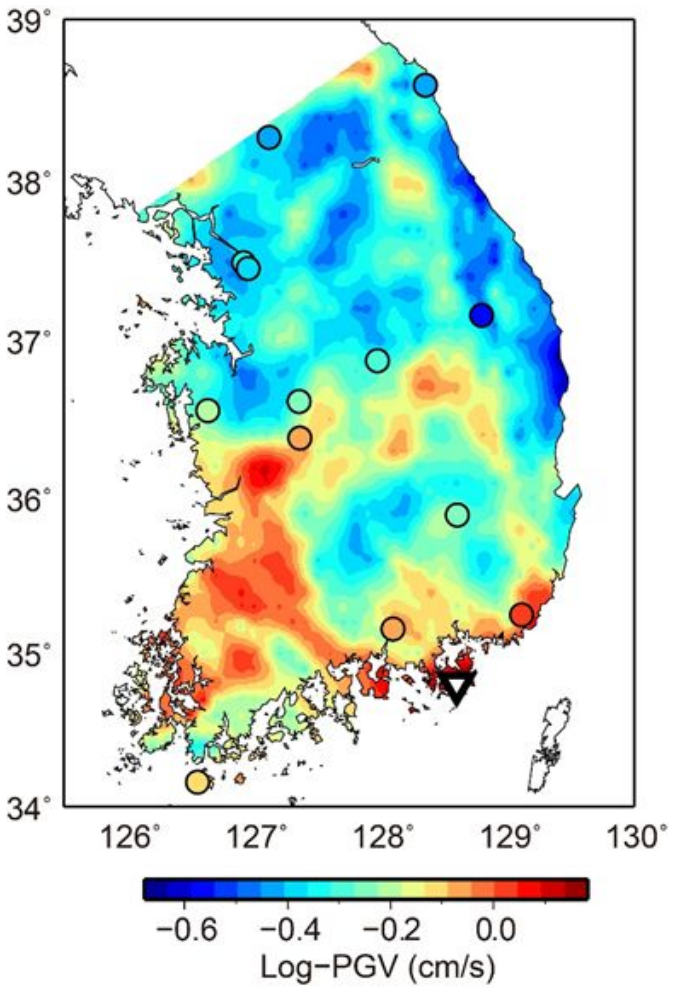

Fig 12. Peak ground velocity values across the Korean Peninsula for the 2005 Fukuoka earthquake. Synthetic values are colored in the background and station observations are colored in enclosed circles with the same scale. The location of maximum PGV is indicated with the white triangle.

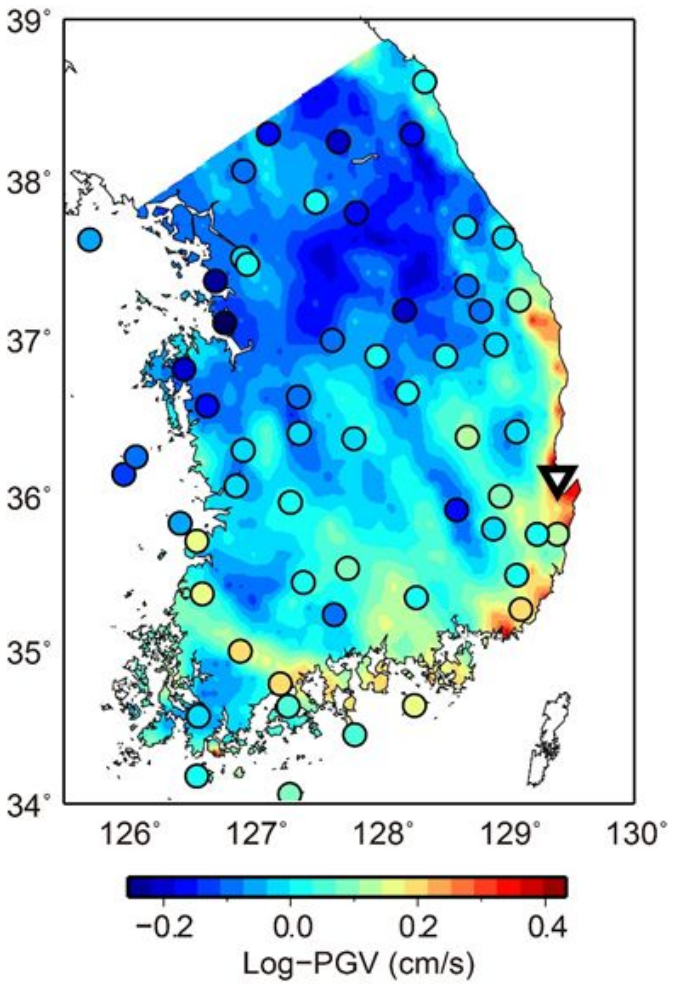

Fig 13. Peak ground velocity values across the Korean Peninsula for the 2016 Kumamoto earthquake. Synthetic values are colored in the background and station observations are colored in enclosed circles with the same scale. The location of maximum PGV is indicated with the white triangle.

3.3 Comparison with Ground Motion Prediction Equations

The computed PGV values are plotted according to distance along with GMPEs (Emolo et al., 2015) for comparison in both 2005 Fukuoka earthquake and 2016 Kumamoto earthquake in **Fig 14** and **Fig 15**. The synthetic PGV values fit the GMPE and lie within the variance boundary, with the exception of few stations far away from the source.

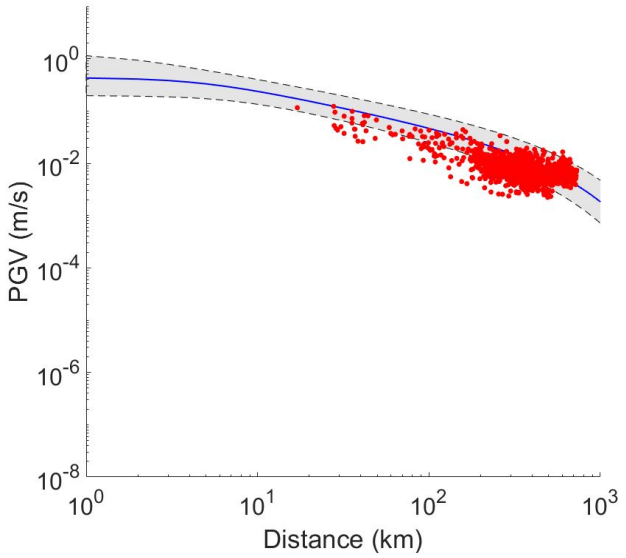

Fig 14. Peak ground velocity values computed across the Korean Peninsula compared with GMPEs for the 2005 Fukuoka earthquake

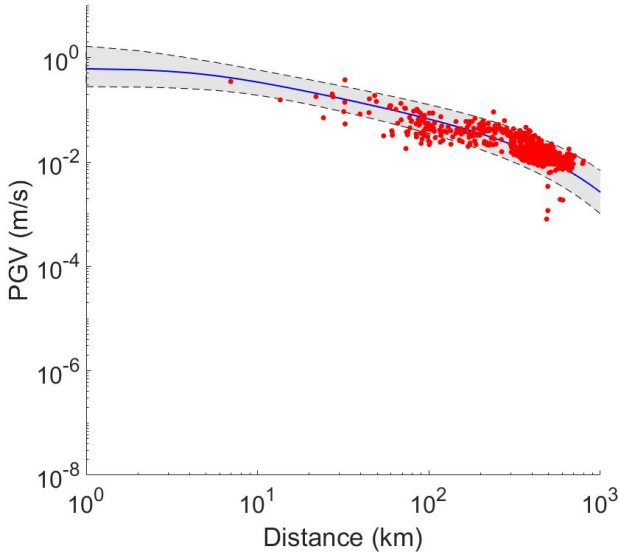

Fig 15. Peak ground velocity values computed across the Korean Peninsula compared with GMPEs for the 2016 Kumamoto earthquake

IV. FURTHER TASKS

4.1 Verification of Waveform Modelling

Having encountered the problem that the velocity seismogram is in discordance with observations at high frequency, further verification of waveform modelling is necessary. The current plan is to compare the synthetic waveform calculated through spectral element method with frequency-wavenumber modelling results. Synthetic seismograms from a point-source solution of the 2016 Kumamoto earthquake with 1D-PREM velocity structure calculated through SPECFEM3D and FKSYN1D will be compared to examine the cause of discordance.

4.2 Pseudo-Dynamic Earthquake Rupture Scenario

The earthquake rupture scenario will be generated based on the rupture model generator code developed by S. G. Song (Song et al., 2014). The rupture model generator emulates the physically consistent rupture process through statistical analysis of dynamic rupture models. 1-point statistics (mean and standard deviation) and 2-point statistics (auto-correlation and cross-correlation) of the earthquake source parameters derived from dynamic rupture models generate slip, peak slip velocity, and rupture velocity as spatial random fields. The generated rupture scenario will be projected onto the finite fault models of major active fault zones located at northern Kyushu. The northern segment of the Kikugawa fault zone or the Oshima-Oki segment of the Nishiyama fault zone are possible candidates for the final fault model for the scenario earthquake, as both fault segments have size capable of creating a Mw 7.0 earthquake and have reasonable chance of rupture.

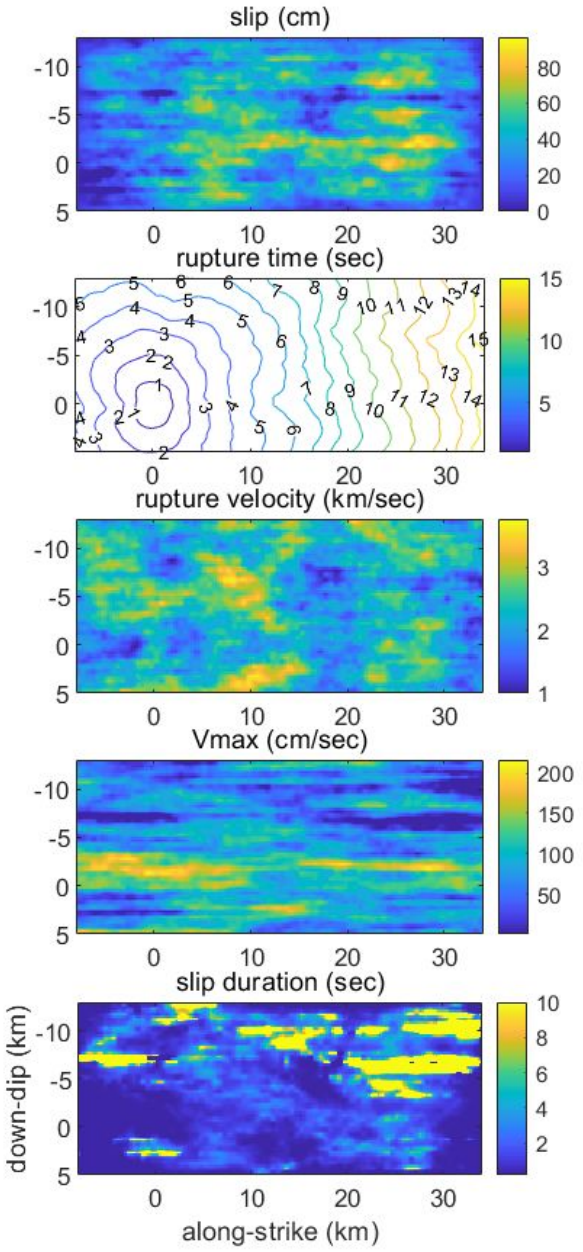

Fig 16. A test case for pseudo-dynamically generated earthquake rupture scenario.

REFERENCES

[1] Andrews, D. J. (1976). Rupture velocity of plane strain shear cracks, J. Geo-phys. Res. 81, no. 32, 5679-5687

[2] Asano, K. and T. Iwata (2006). Source process and near-source ground motions of the 2005 West Off Fukuoka Prefecture earthquake. Earth Planes Space. 58, 93-98

[3] Asano, K. and T. Iwata (2016). Source rupture processes of the foreshock and mainshock in the 2016 Kumamoto earthquake sequence estimated from the kinematic waveform inversion of strong motion data. Earth Planets Space, 68:147

[4] Dalguer, L. A. and P. M. Mai (2011). Near-source ground motion variability from M = 6.5 dynamic rupture simulations, in 4th IASPEI/IAEE International Symposium, University of California, Santa Barbara, USA.

[5] Dalguer, L. A. and P. M. Mai (2012). 2012. Prediction of near-source ground motion exceeding 1 g at low frequencies (<2 Hz) from Mw ~ 6.5 deterministic physics-based dynamic rupture simulations, in Proceedings of the 15th World Conference on Earthquake Engineering (15WCEE), Lisbon, Portugal.

[6] Tinti, E., E. Fukuyama, A. Piatanesi, M. Cocco (2005) A kinematic source-time function function compatible with earthquake dynamics Bulletin of the Seismological Society of America. Vol. 95, No. 4, 1211-1223

[7] Emolo, Antonio Sharma, Nitin & Festa, Gaetano & Zollo, Aldo & Convertito, V & Park, Jung-Ho & Chi, Heon-Cheol & Lim, In-Seub. (2015). Ground-Motion Prediction Equations for South Korea Peninsula. Bulletin of the Seismological Society of America. 105. 10.1785/0120140296.

[8] Komatitsch, D. and J. Tromp (2002). Introduction to the spectral element method for three-dimensional seismic wave propagation. Geophysical Journal International. 139, issue 3, 806-822

[9] Kim, S, H. Tkalčić, J. Rhie, and Y. Chen (2016). Intraplate volcanism controlled by back-arc and continental structures in NE Asia inferred from transdimensional Bayesian ambient noise tomography. Geophysical Research Letters. 43, 8390-8398

[10] Schemedes, J., R. J. Archuleta, and D. Lavallee (2012). A kinematic rupture model generator incorporating spatial interdependency of earthquake

source parameters. Geophys. J. Int. 192, no. 3, 1116-1131

[11] Song, S. G., L. A. Dalguer, and P.M. Mai (2014). Pseudo-dynamic source modelling with 1-point and 2-point statistics of earthquake source parameters. Geophys. J. Int. 196, 1770-1786